Eur. Phys. J. D **12**, 369–375 (2000)

THE EUROPEAN PHYSICAL JOURNAL D

EDP Sciences

Simulation of shifted and asymmetric hydrogen line profiles

S. Sorge[1,a] and S. Günter[2]

[1] Universität Rostock, Fachbereich Physik, Universitätsplatz 3, 18051 Rostock, Germany
[2] Max-Planck-Institut für Plasmaphysik, Boltzmannstraße 2, 85748 Garching, Germany

Received 12 April 2000

Abstract. A theoretical approach to spectral line shapes of hydrogen-like emitters in plasmas has been developed. Within this approach, the line core as well as the line wings are well described. Besides the ion dynamics, shift and asymmetry are also included. The time evolution of the ionic microfield is taken into account by means of a simulation technique. Shift and asymmetry of the lines result from the inclusion of the electronic contributions to the line shift as well as from the inhomogeneities of the ionic microfield and the quadratic Stark effect. Calculated line profiles according to the presented formalism are given for the Lyman-α line and the Lyman-β line of atomic hydrogen in an argon plasma, and compared with results of other theories and corresponding experiments.

PACS. 52.25.Qt Emission, absorption, and scattering of ultraviolet radiation – 32.70.Jz Line shapes, widths, and shifts

1 Introduction

The interaction between hydrogen radiators in dense plasmas and the microfield of the plasma ions leads to a broadening of the hydrogen spectral lines caused by the splitting of the atomic levels due to the linear Stark effect, as well as to shift and asymmetry as a consequence of the interaction between the atomic quadrupole moment and inhomogeneities of the ionic microfield, the so called quadrupole effect, and higher order effects, *e.g.* the quadratic Stark effect. Here, the quadrupole effect causes different shifts of the Stark components which gives the dominant contribution to the line asymmetry [1].

For small deviations $\Delta\omega$ from the unperturbed transition frequency, the times $\tau \sim 1/\Delta\omega$ to be considered are long enough to resolve the motion of the plasma ions. For very narrow lines and near the line centres effects due to the ion motion have to be considered. Experimental investigations of the line centres of the first Lyman lines by Grützmacher and Wende [2,3] demonstrated the importance of inclusion of the dynamics of the ionic microfield. It leads to an additional large contribution to the broadening of spectral lines for lines with a central Stark component, *e.g.* the Lyman-α line, or to a decrease in the depth of the dip in the line centre for lines without a central Stark component, *e.g.* the Lyman-β line. Considering several theoretical approaches, the widths of line shapes calculated by means of computer simulation techniques show the best agreement with experimental data [4,5], whereas calculations without inclusion of the ion dynamics [6,7] or the description of the ion dynamics by several analytic models [8–10] lead to larger discrepancies between experimental and theoretical line profiles near the line centre. On the other hand, using simulation techniques, shift and asymmetry of the spectral lines have been neglected so far [4,5]. Shifted and asymmetric profiles have been calculated only in the frame of analytical descriptions of the plasma ions [6,9,11].

The aim of this work is to improve line profiles achieved by computer simulations, including shift and asymmetry. In the simulation, the ions are considered as independent particles moving along straight trajectories. The shift and asymmetry due to the ionic quadrupole effect has been calculated by means of a field dependent, averaged field gradient as introduced by Chandrasekhar and von Neumann [12] and extended to screened particles by Halenka [13].

Apart from the broadening, shift and asymmetry due to the plasma ions, in our calculations the electronic broadening and shift are included. They are calculated within a quantum statistical approach using a Green's functions technique [14,15].

Furthermore, the so called "trivial" asymmetry and the Doppler broadening due to the motion of the radiators are taken into account.

To test the developed theory, the shapes of the first two Lyman lines are calculated for the plasma parameters chosen in references [2,3] and compared to experimental data.

[a] e-mail: stefans@darss.mpg.uni-rostock.de

2 Theory

In our calculations, we have taken into account the line broadening, shift and asymmetry due to the interaction between a radiating atom and the surrounding plasma particles (so called pressure broadening), the trivial asymmetry, as well as the line broadening due to the motion of the radiators (Doppler broadening). Here, we have calculated first a profile $I^{\rm pr}(\Delta\omega)$ for a radiator at rest, where only the pressure broadening is taken into account. The full line shape $I(\Delta\omega)$ is yielded by including the Doppler broadening *via* convolution of $I^{\rm pr}(\Delta\omega)$ with the Maxwellian velocity distribution function.

For a fixed radiating hydrogen atom in a plasma environment, the shape of an emitted spectral line is given by [16]

$$I^{\rm pr}(\Delta\omega) \propto \exp\left(-\frac{\hbar\Delta\omega}{k_{\rm B}T}\right)\left(1+\frac{\Delta\omega}{\omega^{(0)}}\right)^4 L(\Delta\omega)$$

with the unperturbed transition frequency $\omega^{(0)} = (E_i^{(0)} - E_f^{(0)})/\hbar$ and $\Delta\omega = \omega - \omega^{(0)}$. Here, $L(\Delta\omega)$ includes the effects of shift, broadening and asymmetry due to the interaction between the radiating atom and the plasma particles. The factor apart from $L(\Delta\omega)$ gives the contribution to the asymmetry due to the occupation density of the atomic states of the upper level as well as the trivial asymmetry.

For spectral lines of a dipole transition, $L(\Delta\omega)$ is given by the Laplace transform

$$L(\Delta\omega) = {\rm Re}\frac{1}{\pi}\int_0^\infty {\rm d}t\ {\rm e}^{{\rm i}\Delta\omega t} C(t)$$

of the dipole-autocorrelation function

$$C(t) = e^2 \sum_{i,i',f,f'} \rho_i \langle i|\mathbf{r}|f\rangle\langle f'|\mathbf{r}|i'\rangle\langle i'|\langle f|\langle U(t)\rangle_{\rm av}|f'\rangle|i\rangle\,. \tag{1}$$

In this formula, $\langle ...\rangle_{\rm av}$ denotes the ensemble average over all radiating atoms in the plasma, which are influenced by different time dependent microfields $\mathbf{E}(t)$ during the time interval t. This average may be performed as an average over all possible microfields, acting on a representative radiator. $\mathbf{d} = -e\mathbf{r}$ is the dipole operator of the atomic transition, and $U(t) = U_f^+(t)U_i(t)$ signs the product of the time evolution operators for the states of the initial levels (i) and the final levels (f), respectively. Using the usual no-quenching approximation, *i.e.* performing the summation only over states with the principal quantum number of the upper or lower level of the considered atomic transition, the time evolution operator $U(t)$ satisfies the equation of motion

$$\frac{\rm d}{{\rm d}t}\langle i'|\langle f|U(t)|f'\rangle|i\rangle = -\frac{\rm i}{\hbar}\sum_{i_1,f_1}\langle i'|\langle f_1|\Delta V(t)|f'\rangle|i_1\rangle\langle i_1|\langle f|U(t)|f_1\rangle|i\rangle \tag{2}$$

with the difference between the radiator-plasma interaction potentials for the initial and final states

$$\Delta V(t) = V_i(t) - V_f^+(t) + {\rm i}\Gamma_{if}^{\rm V}.$$

The potentials $V_i(t)$ and $V_f(t)$, containing an electronic self energy and an explicit time dependent ionic potential

$$V_n(t) = V_n^{\rm ion}(t) + \Sigma_n^{\rm e}, \quad n = i, f,$$

act only in the space of the initial states $|i\rangle$ and final states $|f\rangle$, respectively. The term $\Gamma_{if}^{\rm V}$ is the vertex correction to the electronic broadening, describing the coupling between the initial and the final level. It vanishes in the case of the Lyman lines [11].

The electronic contribution may be written as a self energy, calculated within a second-order Born approximation [14,15],

$$\Sigma_n^{\rm e}(E_n/\hbar + \Delta\omega, \beta) = -\frac{1}{e^2}\int\frac{{\rm d}^3q}{(2\pi)^3}V(q)\sum_\alpha |M_{n\alpha}^{(0)}(\mathbf{q})|^2 \times \int_{-\infty}^{\infty}\frac{{\rm d}\omega}{\pi}(1+n_{\rm B}(\omega))\frac{{\rm Im}\varepsilon^{-1}(\mathbf{q},\omega)}{E_n^{(0)} - E_\alpha(\beta) + \hbar\Delta\omega - \hbar(\omega + {\rm i}0)}\,.$$

Here, $V(q)$ is the Coulomb potential, $\varepsilon(\mathbf{q},\omega)$ the dielectric function in random phase approximation, and $n_{\rm B}(\omega)$ the Bose function. $\beta = E/E_0$ is the normalized field strength with the Holtsmark normal field strength [17]

$$E_0 = \frac{e}{2\varepsilon_0}\left(\frac{4n}{15}\right)^{\frac{2}{3}}. \tag{3}$$

In this paper, the frequency dependence of the self energy as well as the field strength dependence of the energies E_α are neglected, *i.e.*

$$\Delta\omega = 0 \quad \text{and} \quad E_\alpha(\beta) \longrightarrow E_\alpha(\beta)\big|_{\beta=0} = E_\alpha^{(0)},$$

corresponding to the impact approximation [16,18]. This is reasonable for the narrow lines considered here, where ion dynamics play an important role.

To calculate the ionic contribution, the effective Hamiltonian

$$V^{\rm ion}(t) = e\mathbf{r}\cdot\mathbf{E}(t) - \frac{1}{2}\sum_{ij}\alpha_{ij}E_i(t)E_j(t) - \frac{1}{6}\sum_{ij}Q_{ij}\langle E_{ij}\rangle_{\mathbf{E}(t)} \tag{4}$$

has been used. The first term is the linear Stark effect with the time dependent ionic microfield $\mathbf{E}(t)$ and the atomic dipole operator $\mathbf{d} = -e\mathbf{r}$. The second term is the quadratic Stark effect with the symmetric tensor of the atomic dipole polarisability α_{ij}. The matrix elements of this contribution are calculated using an expansion of the wave function in wave function which are defined in a coordinate system with the positive z-axis being parallel

to the time dependent microfield $\mathbf{E}(t)$ in every time step, *i.e.*

$$\sum_{ij}\langle nl_1m_1|\alpha_{ij}|nl_2m_2\rangle E_i(t)E_j(t) = \sum_m D^{(l_1)}_{m_1m}(0,\Theta_{\mathbf{E}},\varphi_{\mathbf{E}}) \times \langle nl_1m|\alpha_{zz}E^2(t)|nl_2m\rangle D^{(l_2)}_{m,m_2}(-\varphi_{\mathbf{E}},-\Theta_{\mathbf{E}},0).$$

Here,

$$D^{(l)}_{m'm}(\alpha,\beta,\gamma) = \langle lm'|\exp\left(\frac{\mathrm{i}\gamma}{\hbar}J_z\right)\exp\left(\frac{\mathrm{i}\beta}{\hbar}J_y\right)\exp\left(\frac{\mathrm{i}\alpha}{\hbar}J_z\right)|lm\rangle$$

[19] are the matrix elements of finite rotations expanding the spherical wave functions $|lm\rangle$ defined in the coordinate system Σ in spherical wave functions $|lm'\rangle$ defined in the coordinate system Σ', where Σ' is rotated by the Euler angles α,β,γ compared to Σ. $\varphi_{\mathbf{E}}$ and $\Theta_{\mathbf{E}}$ are the field angles in our fixed coordinate system Σ'. In this equation, the matrix elements of α_{zz} are represented by

$$\langle nl_1m|\alpha_{zz}|nl_2m\rangle = \sum_{n_1n_2}\langle nl_1m|n_1n_2m\rangle\alpha_{zz,n_1n_2m}\langle n_1n_2m|nl_2m\rangle$$

with the hydrogen wave functions $|n_1n_2m\rangle$ calculated in parabolic coordinates [20]. n_1, n_2 are the parabolic quantum numbers, and m is the magnetic quantum number, being related to the principal quantum number n by

$$n = n_1 + n_2 + |m| + 1.$$

The resulting expressions for the dipole polarisability read

$$\alpha_{zz,n_1n_2m} = \frac{n^4}{8}\left(17n^2 - 3(n_1-n_2)^2 - 9m^2 + 19\right)4\pi\varepsilon_0 a_{\mathrm{B}}^3.$$

The last term in equation (4) describes the interaction between the atomic quadrupole moment and the inhomogeneities of the electric field. Here, $Q_{ij} = -e(3r_ir_j - \delta_{ij}r^2)$ is the atomic quadrupole operator, and

$$E_{ij} = \frac{\partial E_i(\mathbf{R})}{\partial R_j} - \frac{1}{3}\delta_{ij}\nabla\cdot\mathbf{E}(\mathbf{R})\bigg|_{R=0}$$

is a traceless tensor, which in the following is called the field gradient. For a Debye-screened electric field, it is given by [13]

$$E_{ij} = -\sum_a \frac{q_a}{4\pi\varepsilon_0 R_a^3}\mathrm{e}^{-\frac{R_a}{r_{\mathrm{D}}}} \times\left(1+\frac{R_a}{r_{\mathrm{D}}}+\frac{R_a^2}{3r_{\mathrm{D}}^2}\right)\left(3\frac{R_{a,i}R_{a,j}}{R_a^2}-\delta_{ij}\right)$$

with the Debye screening length $r_{\mathrm{D}} = (\varepsilon_0 k_{\mathrm{B}}T/n_{\mathrm{e}}e^2)^{1/2}$. From that, the averaged field gradient for a given microfield [13]

$$\langle E_{ij}\rangle_{\mathbf{E}} = -\frac{5}{\sqrt{32\pi}}\frac{E_0}{R_0}B_\rho(\beta)A_{ij}(\mathbf{E}/E)$$

is found, where $B_\rho(\beta)$ is the normalized averaged field gradient, being a generalization of the function $B(\beta)$ of Chandrasekhar and von Neumann [12] within the Baranger-Mozer limit [21,22]. R_0 is the next neighbour distance, which is related to the Holtsmark normal field strength (3) by $E_0 = e/(4\pi\varepsilon_0 R_0^2)$, and $\rho = R_0/r_{\mathrm{D}}$ is a screening parameter. The dependence of $\langle E_{ij}\rangle_{\mathbf{E}}$ on the direction of the field $\mathbf{E}$ is given by the coefficients

$$A_{ij}(\mathbf{E}/E) = 3\,\frac{E_iE_j}{E^2} - \delta_{ij}, \quad i,j = 1,2,3.$$

3 Simulation procedure

The dipole-autocorrelation function $C(t)$ (1) has been determined by solving the equation of motion (2) numerically with simulated ionic microfields, using a Runge-Kutta-Merson method [23]. To generate the time dependent microfields, we have simulated the motion of 1000 test ions, neglecting any correlation between the particles, so that the ions are moving along straight trajectories. For the simulation volume, we have chosen a cubic box with an edge length $l = 10/n_{\mathrm{e}}^{1/3}$. The ions produce Debye-screened electric fields. Only the plasma electrons are assumed to contribute to the screening. Contributions to the electric field due to ions outside of the box have been neglected. The ion velocities satisfy the Maxwellian velocity distribution. An ion, leaving the simulation volume, is replaced by a new one according to periodic boundary conditions at the opposite of the box, moving with the same velocity and in the same direction [24].

The radiating atom is fixed in the centre of the box. To reproduce the relative motion of a radiator-perturber pair, we have used the so called μ-ion model, *i.e.*, in the velocity distribution, the ion mass is replaced by the reduced radiator-perturber-mass μ.

At the begin of the simulation procedure, the ions are randomly distributed, where the correlation between the ions is completely neglected. This seems to be meaningful, because this correlation becomes lost after the averaged time for one ion impact [4,5]. The initial values for the normalized field strength $\beta = E/E_0$ are situated between 0 and $\beta_{\max}$, where $\beta_{\max} = 100$ for the Lyman-α line, and $\beta_{\max} = 40$ for the Lyman-β line. To get initial field strengths distributed over the whole range, the range has been divided into domains $\Delta\beta$ [25] with $\Delta\beta = 0.1$ for $\beta \le 10$ and $\Delta\beta = 0.5$ for $\beta \ge 10$. For every domain, 10 initial configurations were chosen. The large values of $\beta_{\max}$ are found to be necessary to reproduce the line asymmetry. In particular, a $\beta_{\max}$, being too small, as in the case of Lyman-α profiles with static ions, lead to large discrepancies between asymmetries of the simulated profiles and that calculated within the method from reference [11].

The minimum distance between the radiating atom and the surface of the simulation box is $R_{\mathrm{s}} = 5/n_{\mathrm{e}}^{1/3}$. Under the plasma conditions assumed for the line shape calculations, this is larger than 3 Debye screening lengths r_{D}, suggested in reference [5].

Table 1. Full widths at half maximum (FWHM) for Lyman-α profiles in Å for the conditions of the experiment of Grützmacher and Wende [2]. The hydrogen radiators were in an argon plasma. All profiles include Stark broadening as well as Doppler broadening. The electronic shifts and widths corresponding to the columns no. 4, 5, 6, and 8 are calculated using the method of Günter and Könies (GK) according to reference [15]. Halenka *et al.* [5] have calculated profiles which are only broadened, but not shifted and asymmetric. They have simulated the electronic microfield as well as the ionic one.

n_e [10^{23} m^{-3}]	T [K]	experiment	static ions (GK)	static ions (simulation)	MMM	dyn. ions simulation Halenka *et al.*	dyn. ions simulation this work
1.0	12700	0.23 ± 0.02	0.144	0.144	0.183	0.221	0.211
2.0	13200	0.30 ± 0.02	0.172	0.176	0.234	0.287	0.278
3.0	13200	0.36 ± 0.02	0.207	0.209	0.286	0.358	0.332
4.0	14000	0.42 ± 0.02	0.241	0.242	0.337	0.426	0.387

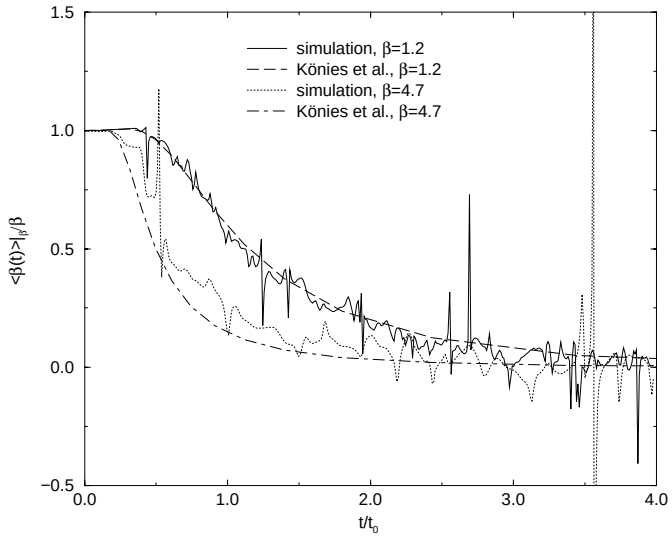

Fig. 1. Simulated conditional covariance (Eq. (5)) compared to that calculated with the approach of Könies *et al.* [28]. Here, the screening parameter is $\rho = R_0/r_D = 0.612$, corresponding to $T = 10\,000$ K and $n_e = 10^{23}$ m^{-3}.

The initial fields satisfy the field distribution function $W(E) = 4\pi W(\mathbf{E})$ for Debye-screened, uncorrelated ions, and the simulated microfields reproduce the field-autocorrelation function for a given initial field strength, the so called conditional covariance [26,27]

$$\gamma(t|E) = \frac{1}{E^2} \int \mathrm{d}^3F \; \frac{\mathbf{F}\cdot\mathbf{E}\; W_2(\mathbf{F},t;\mathbf{E},0)}{W(\mathbf{E})}, \qquad (5)$$

calculated by Könies *et al.* [28]. They also have calculated this property within the μ-ion model for Debye-screened, uncorrelated particles with the charge e. In this formula, $W_2(\mathbf{F},t;\mathbf{E},0)$ is the two-time field distribution function. Figure 1 shows our simulated conditional covariance compared to that of Könies *et al.*, plotted over the normalized time $\tau = t/t_0$ with

$$t_0 = \sqrt{\frac{\mu}{2k_B T}} R_0.$$

The conditional covariance depends only on the parameters $\rho = R_0/r_D$ and $\beta = E/E_0$, as shown in [28]. We have chosen $\rho = 0.612$, according to a plasma with a density $n = 10^{23}$ m^{-3} and a temperature $T = 10\,000$ K. Our initial fields were $\beta = 1.2$ and $\beta = 4.7$. For this work, it has been simulated with 50 000 initial configurations. Despite this high number, the fluctuations are much larger than those of the corresponding dipole-autocorrelation function $C(t)$.

4 Results

Within the formalism outlined in the previous sections, full line profiles $I(\Delta\lambda)$ of the Lyman-α line and the Lyman-β line for atomic hydrogen are calculated, where pressure broadening and trivial asymmetry, as well as Doppler broadening are included. $\Delta\lambda$ is the deviation from the wave length of the radiation of an unperturbed atomic transition $\lambda^{(0)} = 2\pi c\hbar/(E_i^{(0)} - E_f^{(0)})$. From these profiles, the width, shift and asymmetry were determined. Here, the centre-of-mass shift

$$\Delta^{\mathrm{cm}} = \frac{\int_{-\Delta s}^{\Delta s} \mathrm{d}(\Delta\lambda)\, \Delta\lambda\, I(\Delta\lambda)}{\int_{-\Delta s}^{\Delta s} \mathrm{d}(\Delta\lambda)\, I(\Delta\lambda)} \qquad (6)$$

and the asymmetry parameter

$$A(\Delta\lambda) = \frac{I^{\mathrm{red}}(\Delta\lambda) - I^{\mathrm{blue}}(\Delta\lambda)}{I^{\mathrm{red}}(\Delta\lambda) + I^{\mathrm{blue}}(\Delta\lambda)}, \qquad (7)$$

with $I^{\mathrm{red}}(\Delta\lambda) = I(|\Delta\lambda|)$ and $I^{\mathrm{blue}}(\Delta\lambda) = I(-|\Delta\lambda|)$ were determined, according to reference [3]. The shift Δ^{cm} has been calculated only for the Lyman-α profiles, where we have chosen $\Delta s = 1.5$ Å according to reference [15].

To allow comparisons with experimental results, the plasma conditions from the experiments of Grützmacher and Wende in references [2,29], and [3], respectively, were chosen.

Because of the small width of the Lyman-α line, the whole line profile is determined by the dynamics of the ionic microfield. In Table 1, the full width at half maximum (FWHM) of the Lyman-α profiles is given for several plasma conditions and yielded by different theoretical approaches, compared to those of the experiment [2]. The neglect of the dynamics of the ionic microfield leads

Table 2. Centre-of-mass shift Δ^{cm} from equation (6) of the Lyman-α line for $n_{\mathrm{e}} = 2 \times 10^{23}$ m^{-3} and $T = 13\,200$ K according to the plasma conditions of the second line in Table 1. The integration interval was $[-\Delta s, \Delta s]$ with $\Delta s = 1.5$ Å, according to reference [11]. The experimental value is from reference [29].

method	experiment	static ions (GK)	static ions (simulation)	MMM	dyn. ions simulation this work
shift [10^{-3} Å]	(5.8 ± 0.6)	3.35	3.73	4.09	7.11

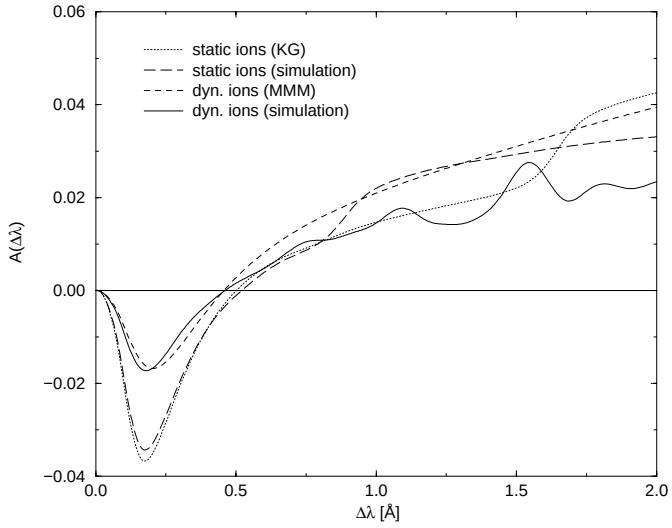

Fig. 2. Asymmetry $A(\Delta\lambda)$ of calculated Lyman-α profiles according to equation (7) of hydrogen atoms in an argon plasma of $n_{\mathrm{e}} = 2 \times 10^{23}$ m^{-3} and $T = 13\,200$ K according to the second line in Table 1. The asymmetry has been calculated regarding to the position of the maximum.

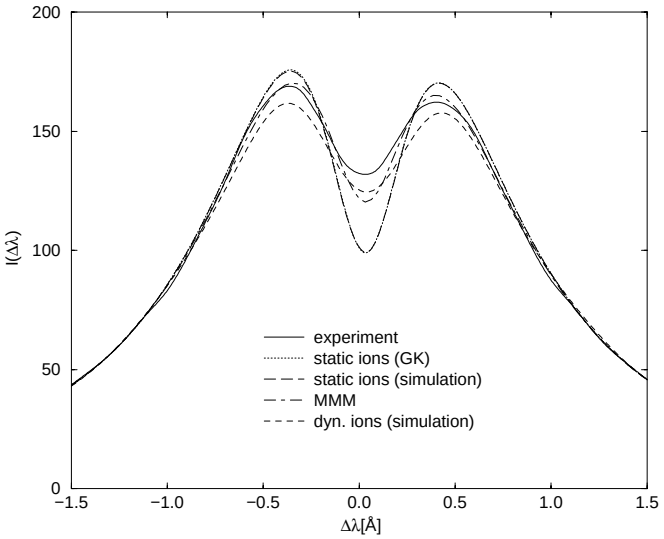

Fig. 3. Profiles of the Lyman-β line of hydrogen for $T = 16\,000$ K and $n_{\mathrm{e}} = 2 \times 10^{23}$ m^{-3} according to Table 3.

to a strong underestimation of the width of the Lyman-α line. The use of several analytical models and approaches have yielded a better agreement between theoretical and experimental line shapes. For comparison, we have chosen the width of the profiles, where the ion dynamics are taken into account by a stochastic model, the model-microfield method [26,27,30]. But all these approaches still underestimate the effects due to the dynamic ionic microfield. Up to now, profiles yielded from simulation techniques, show the best agreement with experimental line shapes with respect to the width as a consequence of the most realistic description of the ionic microfield. Here, our approach leads to a slight underestimation of the width. This underestimation is probably a consequence of the use of electronic widths in impact approximation. Halenka *et al.* [5] have compared the widths of the Lyman-α profiles, where both the ionic and the electronic microfield has been simulated, with others, where the electronic widths were calculated in impact approximation. Using the first method, the widths of the resulting profiles agree well with those of the measured profiles. The widths of the profiles, calculated using the second method, were about 5% smaller. The inclusion of the ion dynamics within our simulation technique results in an increase of the red shift of the line shapes, as shown in Table 2, and a decrease of the line asymmetry, seen in Figure 2, compared to that of the static ion profiles. Here, only theoretical curves are plotted because no experimental data were available. Both effects may be explained by the suppression of the quadrupole effect due to the time evolution of the ionic microfield, particularly due to rotations of the microfield. These rotations of the ionic microfield have a stronger influence on the quadrupole effect than on the quadratic Stark shifts. This results in an increase of the red shift of the line profiles, since the field rotations decrease the shifts resulting from both effects. The fluctuations in the asymmetry of the simulated profile in Figure 2 are due to numerical difficulties. The strong increase in the line wings are a consequence of the decrease of the expression $I^{\mathrm{red}}(\Delta\omega) + I^{\mathrm{blue}}(\Delta\omega)$ in the denominator of the asymmetry parameter $A(\Delta\omega)$, which becomes small for wave length deviations larger than the half width at half maximum (HWHM) $\Delta\lambda_{1/2}$. Note, that $\Delta\lambda_{1/2} \sim 0.1$ Å for $n_{\mathrm{e}} = 2 \times 10^{23}$ m^{-3} and $T = 13\,200$ K.

The profile and the asymmetry of the Lyman-β line are only modified by the ion dynamics near the line centre. Figure 3 shows the central region of a Lyman-β profile calculated within our simulation technique compared to a measured line shape of the experiment of Grützmacher and Wende, and to other theoretical line shapes. For the calculations, we have assumed an Ar^+-plasma with $n_{\mathrm{e}} = 2 \times 10^{23}$ m^{-3} and $T = 16\,000$ K, being the conditions of Grützmacher's and Wende's experiment [3]. All profiles agree in the line wing, where the intensity is mostly

Table 3. Depth of the central dip of the Lyman-β line. The experimental profile is from reference [3], the profile with static ions is calculated using the method of Günter and Könies (GK) from references [11,15]. The simulated profiles were calculated using the simulation technique presented in this work. All theoretical profiles have been calculated using the Hamiltonian of reference [11].

method	experiment	static ions (GK)	static ions (simulation)	MMM	dyn. ions simulation (this work)
depth of the dip	21.9%	43.6%	43.6%	29.2%	22.7%

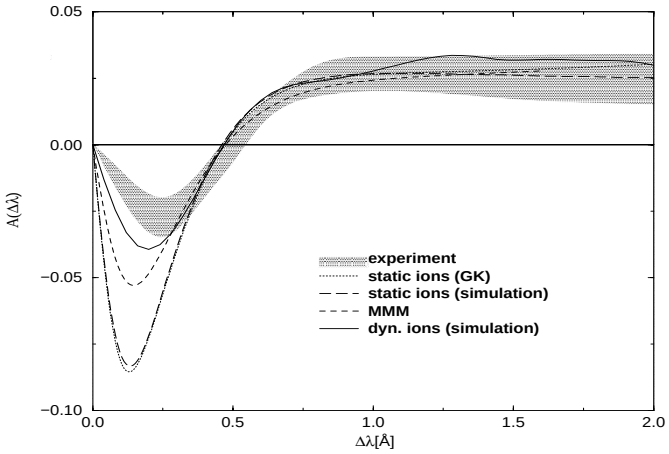

Fig. 4. Asymmetry $A(\Delta\lambda)$ of the Lyman-β profiles over the wave length deviation according to Table 3. The profiles have a full width at half maximum (FWHM) of 1.0 Å. The dotted area indicates the range where the asymmetry curves of the line profiles yielded in the experiment from reference [3], for $n_e = (1.2 \ldots 3.0) \times 10^{23}$ m^{-3} and $T = (12\,700 \ldots 16\,000)$ K are located.

determined by the static Stark splitting. In contrast, the different ways to include the dynamics of the ionic microfield in the calculations lead to significant differences between the profiles near the line centre. Especially, the depth of the central dip depends strongly on the ion dynamics, as shown in Table 3. Here, the inclusion of the ion dynamics within the simulation technique lead to an excellent agreement to the dip-depth of the measured line shape. The asymmetry curves $A(\Delta\lambda)$ of the line shapes, shown in Figure 4, have a similiar behaviour. The positions $\Delta\lambda_0$ of the crossover points, where $I^{\mathrm{red}}(\Delta\lambda_0) = I^{\mathrm{blue}}(\Delta\lambda_0)$, are close to that of the measured profile. For wave length deviations $\Delta\lambda > \Delta\lambda_0$, the asymmetry curves of all calculated profiles are inside the gray area, where the asymmetry curves of all Lyman-β profiles, measured by Grützmacher and Wende for $n_e = (1.2...3.0)\times 10^{23}$ m^{-3} and $T = (12\,700...16\,000)$ K [3], are located. The fluctuations are again due to numerical uncertainties, but are much smaller compared to those of the Lyman-α line since the intensity in the wings of the Lyman-β line is much higher. The inclusion of ion dynamics in the line shape calculations leads to a better agreement between the theoretical and experiamental asymmetry curves, where the best agreement is obtained by means of our simulation technique due to the most realistic description of the dynamic ionic microfield.

5 Conclusions

For the plasma parameters of the experiments described in [2,3,29], line profiles of the Lyman-α and Lyman-β line of atomic hydrogen including ion dynamics as well as shift and asymmetry have been calculated. The time evolution of the ionic microfield has been taken into account within a simulation technique. The use of the simulation leads to a much better agreement between experimental and theoretical line profiles, especially in the line centre, compared to all other theoretical approaches. Shift and asymmetry have been reached by means of an effective Hamiltonian in the equation of motion (2) for the time evolution operator $U(t)$, allowing the calculation of shift and asymmetry while using the no-quenching approximation in the line shape calculations. Apart from the usual linear Stark effect depending on the dynamic ionic microfield, and leading to the ionic line broadening, this Hamiltonian contains an electronic self energy in impact approximation, contributing to the line broadening and shift, as well as explicit expressions for the quadrupole effect and the quadratic Stark effect of the ionic microfield, giving rise to the ionic shift and asymmetry.

We thank G. Röpke for helpful discussions. This work has been supported by the Sonderforschungsbereich 198 "Kinetik partiell ionisierter Plasmen".

References

1. G.V. Sholin, Opt. Spectrosc. (USSR) **26**, 275 (1969).
2. K. Grützmacher, B. Wende, Phys. Rev. A **16**, 243 (1977).
3. K. Grützmacher, B. Wende, Phys. Rev. A **18**, 2140 (1978).
4. V. Cardeñoso, M.A. Gigosos, J. Phys. B: At. Mol. Phys. **20**, 6005 (1987); M.A. Gigosos, V. Cardeñoso, Phys. Rev. A **39**, 5258 (1989).
5. J. Halenka, W. Olchawa, J. Quant. Spectrosc. Radiat. Transfer **56**, 17 (1996).
6. M.E. Bacon, J. Quant. Spectrosc. Radiat. Transfer **17**, 501 (1977).
7. C.R. Vidal, J. Cooper, E.W. Smith, Astrophys. J. Suppl. Ser. **25**, 37 (1973).
8. R.L. Greene, J. Quant. Spectrosc. Radiat. Transfer **27**, 639 (1982).
9. S. Günter, Habilitation thesis, Rostock, 1996.
10. J. Seidel, reference [23] in [3] (private communication with the author).
11. A. Könies, S. Günter, J. Quant. Spectrosc. Radiat. Transfer **52**, 825 (1994).

12. S. Chandrasekhar, J. von Neumann, Astrophys. J. **97**, 1 (1943).
13. J. Halenka, Z. Phys. D **16**, 1 (1990).
14. S. Günter, L. Hitzschke, G. Röpke, Phys. Rev. A **44**, 6834 (1991).
15. S. Günter, A. Könies, J. Quant. Spectrosc. Radiat. Transfer **52**, 819 (1994).
16. H.R. Griem, *Spectral line broadening by plasmas* (Academic press, New York and London, 1974).
17. G. Traving, in *Plasma diagnostics*, edited by W. Lochte-Holtgreven (North-Holland Publishing Company, Amsterdam, 1968).
18. H.R. Griem, Phys. Rev. A **28**, 1506 (1983).
19. A.R. Edmonds, *Angular momentum in quantum mechanics* (Princeton UP, Princeton, 1960).
20. L.D. Landau, E.M. Lifschitz, *Lehrbuch der theoretischen Physik* (Akademie Verlag, Berlin, 1979), Vol. 3.
21. M. Baranger, B. Mozer, Phys. Rev. **115**, 521 (1959).
22. B. Mozer, M. Baranger, Phys. Rev. **118**, 3 (1960); *ibid.* 626 (1960).
23. NAG fortran library Mark 15, *Modern numerical methods for ordinary differential equations*, edited by G. Hall, J.M. Watt (Clarendon Press, Oxford, 1976), p. 59.
24. R. Stamm, D. Voslamber, J. Quant. Spectrosc. Radiat. Transfer **22**, 599 (1979).
25. R. Stamm, E.W. Smith, B. Talin, Phys. Rev. A **30**, 2039 (1984).
26. J. Seidel, Z. Naturforsch. **32a**, 1195 (1977).
27. J. Seidel, Z. Naturforsch. **35a**, 679 (1980).
28. A. Könies, S. Günter, G. Röpke, J. Phys. B: At. Mol. Opt. Phys. **29**, 6091 (1996).
29. K. Grützmacher, B. Wende, in *Spectral line shapes*, edited by B. Wende (de Gruyter & Co. Berlin, New York, 1987), Vol. 4, p. 527.
30. A. Brissaud, U. Frisch, J. Quant. Spectrosc. Radiat. Transfer **11**, 1767 (1971).